Measurement of absolute charge-exchange cross sections for He^{2+} collisions with He and H_2

R. J. Mawhorter,[1,2] J. B. Greenwood,[3] A. Chutjian,[1] T. Haley,[2] C. D. Mitescu,[2] and J. Simcic[1]
[1]*Jet Propulsion Laboratory, California Institute of Technology, Pasadena, California 91109, USA*
[2]*Department of Physics and Astronomy, Pomona College, Claremont, California 91711, USA*
[3]*Physics Department, The Queen's University, Belfast BT7 1NN, United Kingdom*
(Received 17 June 2011; published 15 November 2011)

Reported are total, absolute charge-exchange cross sections for collisions of $^3He^{2+}$ ions with He and H_2. Measurements are reported at fixed energies between 0.33 and 4.67 keV/amu. Both the present results and earlier results of others are analyzed in terms of available experimental small-angle differential cross sections as a function of collision energy, and hence the geometry of the exit aperture of the gas-collision cells used by the various experimental groups. In addition, the effective length of gas-collision cells is studied using fluid dynamic and molecular flow simulations to address the density patterns near the cell entrance and exit apertures. When small acceptance-angle corrections were applied, the results of present and previous measurements for the single electron capture in these systems were brought into good accord in the relevant energy ranges. Taken in their entirety, the present data for $^3He^{2+}$ with He and H_2 lend themselves to new theoretical calculations of the multichannel charge-exchange cross sections.

DOI: 10.1103/PhysRevA.84.052714 PACS number(s): 34.50.Gb, 82.30.Fi, 96.60.Vg

I. INTRODUCTION

Charge exchange (CE) of highly charged ions (HCIs) with neutral atomic and molecular species is a dominant process that occurs in a variety of high electron temperature plasmas [1–11]. These plasmas include fusion devices [12–14], as well as plasmas in astrophysical regions that involve the interaction of HCIs with cometary neutral species [15–18], circumstellar neutral clouds [19], and a wide variety of solar system planetary atmospheres and objects [20–22].

The relatively simple, fully stripped helium nucleus (He^{2+}) is second in abundance to protons in the solar wind, and is a factor ∼70 times more abundant than the heavier, metallic species [23]. Molecular hydrogen also comprises 80−95% of the atmosphere of the outer planets [24] where solar-wind and magnetospheric ion interactions lead to x rays via charge exchange. Helium makes up about 10% of interstellar gas and 3−20% of the atmosphere of the outer planets. It has been estimated that the solar-wind interaction with He gives rise to as much as 50% of the total soft x-ray background of the interplanetary region [25].

The rationale for study of the fundamental systems He^{2+}–He and He^{2+}-H_2 is to provide total cross sections for plasma simulation studies, to understand the energy dependence of the absolute CE cross sections, and to address the important topics of angular collection efficiency and effects of gas flow in gas-collision cells. The kinematics involving these light ions, and especially the exothermic nature of the He^{2+}-He interaction provide a rigorous test of the standard ion-beam–gas-cell technique. In the present work detailed knowledge of the flow conditions for the known gas-cell geometry, coupled with the availability of experimental cross sections enable one to make a direct and clearer comparison among the several available total CE cross sections for the collision partners studied here.

II. EXPERIMENTAL CONSIDERATIONS

The present study makes use of the electron cyclotron resonance (ECR) ion source and the CE–x-ray detection beam line at the JPL Highly Charged Ion Facility [26]. Details of the beam lines, the CE geometry, system calibration, data acquisition system, and an error analysis (taking into account statistical errors, errors in the gas target density, ion-current ratios, and absolute currents) have been given in Refs. [1–10]. Two of the error sources are discussed herein in detail through additional studies and simulations. The first is the effect on the measured CE cross sections of the diameter of the gas-cell exit aperture and the resulting charge-exchanged ion collection efficiency ε. The $^3He^{2+}$−He, H_2 CE cross sections are measured with various diameters of exit apertures. Exit apertures of diameters $a = 1.27$, 2.54, and 4.09 mm were used. For the geometric cell length $L = 60.8$ mm, these correspond to aspect ratios $A = L/a = 47.9$, 23.9, and 14.9, respectively, and to collection half-angles $\theta = \tan^{-1}(a/2L) = 0.60^\circ$, 1.20°, and 1.93°, respectively.

The second parameter studied is, via simulation, the gas flow within the target cell, especially the alterations to the path length and gas density along the ion-neutral interaction path arising from gas streaming at the entrance and exit apertures. Exploring different entrance and exit aperture sizes and combinations (e.g., having the x-ray exit port on the collision cell either open or sealed) [27,28] has enabled a more stringent test of the absolute gas-cell pressure calibration. The resulting capacitance manometer-to-cell pressure correction factors from this study were found to be consistent with those determined previously [4].

A systematic approach to the problem of system acceptance angles and angular collection efficiencies of gas cells is made possible by knowledge of small-angle differential cross sections (DCSs) for the nearly equivalent systems of $^4He^{2+}$ + He [29] and $^4He^{2+}$ + D_2 [30]. Bordenave-Montesquieu and Dagnac (hereafter referred to as B-MD) could resolve the signals for individual state-to-state charge-exchange processes, and so did not need to use (as was done in the present work) the $^3He^{2+}$ isotope ion to avoid admixture with background H_2^+ ions of the same mass (m) to charge (q) ratio of $m/q = 2$. B-MD did, however, use D_2 to provide a heavier scattering target for their $^4He^{2+}$ beam, as compared to H_2 in this study.

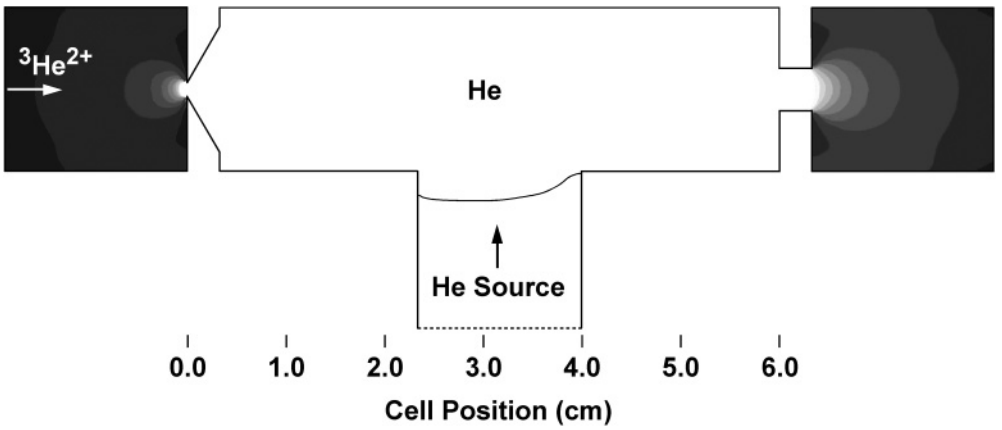

FIG. 1. Results of FLUENT pressure contour calculations for the geometry of the present gas cell. The cell length of 60.8 mm is measured between the exterior cell faces as shown. The cell has a 1.27-mm-diameter knife-edge entrance aperture (left) and a 4.09 mm exit aperture of length 3.18 mm. There are 20 steps in the gray scale from black to white covering a range of pressures from 0 to 1 Pa.

In either case, working with fully stripped He^{2+} projectiles precludes HCI ion source concerns about the presence of metastable states. This fact, coupled with the detailed knowledge of the DCSs for individual states of these few-electron systems, allows one to diagnose with good reliability angular collection and gas-cell streaming effects in measuring benchmark total CE cross sections.

III. THEORETICAL METHODS AND SIMULATIONS

A. Characterizing the effective cell length

The present concern and focus on the gas cell prompted two further studies of the effective length of the cell as experienced by the ion beam. Previous studies [31,32] indicate that for gas cells with reasonably large aspect ratios ($A \geqslant 10$), the additional scattering from the extra-cell gas flowing out of the entrance and exit apertures is almost exactly balanced by the reduction in scattering due to lower pressure inside the cell near these orifices. In other words, $\alpha = L_{\rm eff}/L \approx 1$ is a good approximation. This was predicted by Mathur *et al.* [31], and verified experimentally by Blaauw *et al.* [32] who varied the cell length by a factor of 3 and the cell pressure from 0.4 to 4 Pa. Measured values of total *e*-He cross sections were consistent with $\alpha = 1.00$ and an uncertainty in $L_{\rm eff}$ of 1%.

Access to the sophisticated numerical fluid dynamics software package FLUENT [33] allows one to visualize this gas-streaming effect for the specific cell geometry used here (see Fig. 1). Results of the FLUENT simulation are shown in Fig. 2 in terms of the pressure of helium along the cell axis. Because of the cell cylindrical symmetry a two-dimensional calculation was carried out [34] on an approximately 50 000 cell triangular mesh. The inlet cell pressure was taken as 1.0 Pa. Note that while the larger exit aperture is necessary to allow for good collection efficiency, its thickness helps lead to a compensating lowering of the cell conductance and gas flow at this end. The resulting correction factor $\alpha = 1.030$ agrees well with both the analytical [31] and experimental [32] results. Our present independent assessment is most useful, since it is customized to the cell length and aperture sizes used in these and other CE measurements. It has also provided a framework for including measured angular distributions of the outgoing ions [29,30]. The previous experimental work dealt with electrons [32], and there the final correction factor relied in part on theoretical estimates of differential cross sections for inelastically scattered electrons.

For the CE experiments undertaken here, lower cell pressures—into the molecular flow regime of 2.5×10^{-5} mbar (2.5×10^{-3} Pa)—were used to ensure single-collision conditions. An independent first-order calculation [35] assuming molecular flow [$P < 10^{-3}$ mbar (0.1 Pa)] and aspect ratio $A \geqslant 10$ applied to a cylindrically symmetric cell with 4.09 mm diameter entrance and exit apertures gave $\alpha = 1.010$, in good agreement with the FLUENT value of 1.030. This result at the lower pressure confirms the basic idea that the effective scattering length $L_{\rm eff}$ is essentially equal to the actual cell length L over a wide range of gas-cell pressures.

One can also evaluate the amount of scattering which occurs outside the cell before the entrance aperture and after the exit aperture. In the molecular flow model just described, approximately 6% of the scattering came from outside the cell, and the remaining 94% from within. This compares well

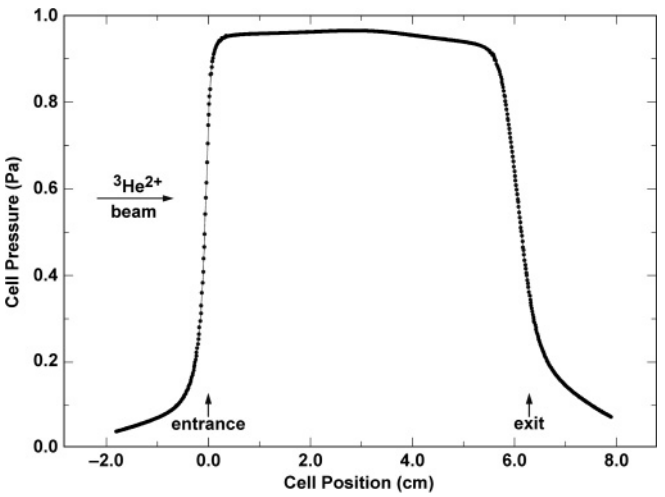

FIG. 2. Pressure data along the cell axis for the FLUENT calculation shown in Fig. 1. The inlet pressure is 1 Pa.

with the simulation results for the present gas cell obtained using FLUENT 5.0 and a kinetic theory viscous model. These yielded 7% outside scattering for the knife-edge inlet, and 11% for the half cell with the larger aperture that is more directly comparable to the cell with end-for-end symmetry described above. The values were derived by integrating along the cell axis (Fig. 2) with linear extrapolations to zero pressure at each end. At 1 Pa the mean free path is comparable to the exit diameter, so it is to be expected that collisions with atoms flowing outward sweep somewhat more gas out of the cell than in a molecular flow model where the mean free path is much longer.

B. Modeling gas-cell collection efficiency with differential cross sections

Small-angle DCSs were measured at beam energies of 2, 4, 6, and 8 keV for $^4He^{2+} + {}^4He$ [29]; and at 4, 6, and 8 keV for $^4He^{2+} + D_2$ [30]. In the entrance channel, before the electron is transferred, there is a weak polarization-potential interaction which results in negligible deflection of the incoming ion. In the exit channel, strong Coulomb repulsion accounts for the angular scattering in the collision, for which a Rutherford scattering description is appropriate [36]. As a result the scattering angle θ depends solely on the impact parameter. As noted above, B-MD were able to resolve energetically several distinct processes in each case. The resulting DCSs are expressed as parametrized graphs of ρ vs τ, where $\rho = (d\sigma/d\Omega)\ \theta\ \sin\theta$ (cm^2) and $\tau = E\theta$ (keV deg). Following this analysis [29], the general integral $\iint (d\sigma/d\Omega) d\Omega$ becomes $\sigma = 2\pi \int (\rho/\tau) d\tau$, assuming no azimuthal angle φ dependence. To obtain a partial cross section for single capture over a parametrized angular range $\{0, \tau_0\}$ one simply integrates using these limits. The total cross section σ_{total} for each process is given by integrating out to the upper limit of πE. In carrying out the integrals, measured DCSs for each process were summed and then represented piecewise by power-law and quadratic functions, as appropriate, and extended to larger angles using a Coulomb line-shape curve varying as K/τ^2 [29]. Here K is a constant used to match the calculated curve to the measured DCS for the process under consideration.

In order to model the collection efficiency ε of a particular gas-cell design, n points are placed along the cell axis at evenly spaced intervals from the entrance aperture to the exit aperture. Due to the cylindrical symmetry, the acceptance half-angle θ subtended by the exit aperture from each point is calculated and converted to a τ value. Next, the partial cross section is calculated and compared to σ_{total}, providing the specific value of ε, or the fraction of the total scattering that can be collected from each of these positions within the cell. Given that single-scattering conditions apply, the values for the n positions are then averaged to yield the overall cell collection ε for that energy and projectile-target pair. It was found that ten points were sufficient to give converged values of efficiencies to better than 1%. Consistent with the near equivalence of the actual and effective cell lengths discussed above, this model was deemed satisfactory: adding points outside the cell would yield only a small negative correction to the very small fraction of the total scattering (1−2% or less for molecular flow) that occurs before the entrance aperture, which should be partially offset by scattering which takes place after the exit aperture. Although this is a somewhat larger fraction of the scattering, for points close to the inside of the exit aperture the subtended angles are large enough that ε is already smoothly approaching 100% for the cases considered here, as shown below in Sec. IV A.

IV. RESULTS AND DISCUSSION

A. Collection efficiencies

The dependence of ε with acceptance half-angle θ is shown in Fig. 3 for $^4He^{2+} + He$ [29] at three different energies, and for the lowest energy case (4 keV = 1 keV/amu) for $^4He^{2+} + D_2$ [30]. One can see that the extra kick He^{2+} receives in the exothermic scattering collision with He requires reasonably

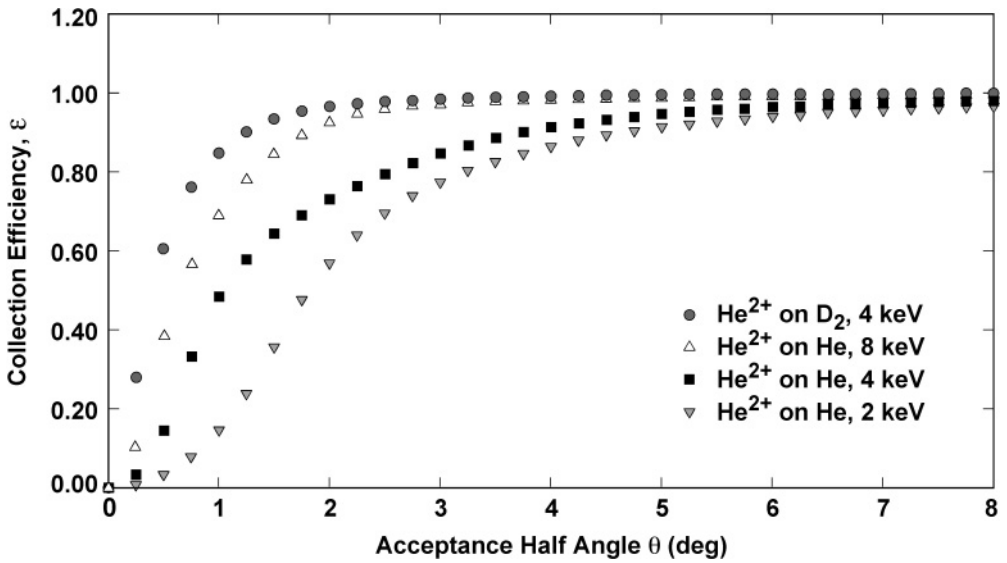

FIG. 3. Collection efficiency ε as a function of acceptance half angle derived from small-angle DCS data for He^{2+} in He and D_2 reported in Refs. [29,30].

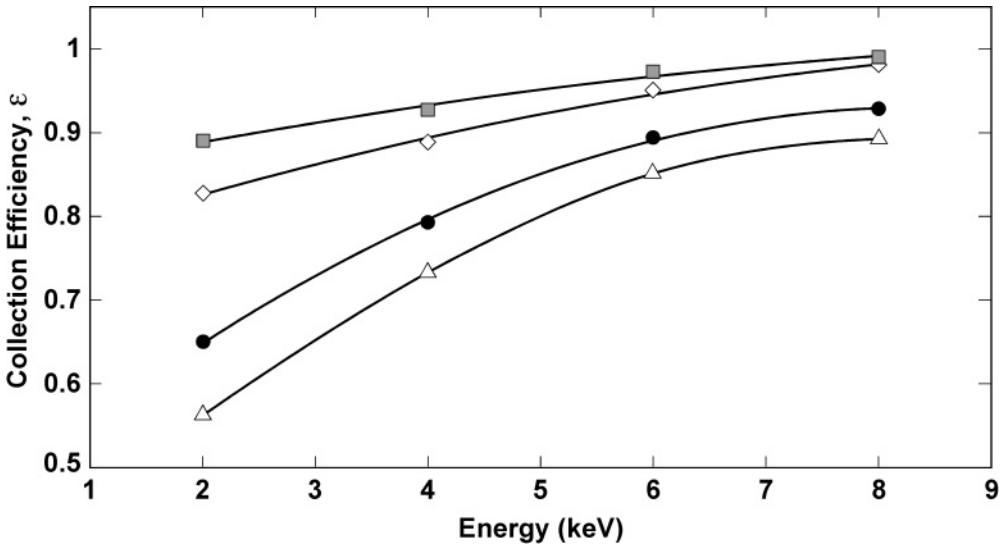

FIG. 4. Collection efficiency ε as a function of He^{2+} projectile energy. Values for ε are calculated from the acceptance-angle data in Fig. 3 applied to gas cells with specific ratios of cell length to exit aperture diameters. Data and acceptance half-angles are ■, Kusakabe *et al.* [38] at 2.50°; ◇, present results at 1.93°; ●, present results at 1.20°; △, Berkner *et al.* [37] at 0.965°.

large acceptance angles, especially at low beam energies. As a result, the He target gives lower collection efficiencies than D_2 for all energies studied herein. Note also that while the ε curves do not cross, their shapes vary with energy. This reflects underlying differen-ces in the measured DCSs that are themselves made up of several processes.

The values of ε for He^{2+} + He for the four different gas cells used in experimental studies are shown in Fig. 4. As discussed above for the present cell geometry, each is characterized by the acceptance half-angle θ from the point at the center of the entrance aperture to the outer edge of the exit aperture. Acceptance angles shown vary from 0.965° for the cell used in the largely higher-energy study of Ref. [37], to 2.50° in the cell used in Refs. [38,39]. The JPL 1.20° and 1.93° acceptance angles lie within these values. In light of the results in Fig. 3, it is perhaps surprising that collection efficiencies are so high. However, these efficiencies are reasonable when one considers that the acceptance angle increases rapidly as the beam approaches the exit aperture, as noted above.

Quadratic energy curves were fitted to each of the four He^{2+} + He energies for each cell geometry, corresponding to the four energies measured by B-MD. These curves were then used to correct the present single-capture cross sections, as well as those of Refs. [37–39]. Use of the JPL 1.20°-apertured cell was only to explore the acceptance-angle issue experimentally. The lowest energy in the study of Ref. [37] was 7.2 keV, and the largest correction actually applied there was approximately 20%.

Another conclusion drawn from Fig. 3 is that the analogous corrections for He^{2+} + H_2 and He^{2+} + D_2 will generally be quite small, on the order of several percent. For the JPL 1.93°-apertured cell the corrections at 1.0, 1.5, and 2.0 keV/amu are 1.3%, 0.5%, and 0.9%, respectively; and correspondingly 0.8%, 0.3%, and 0.6% for Refs. [38,39]. The smallest correction for 1.5 keV/amu is consistent with the measured DCSs of B-MD decreasing most rapidly with τ at this energy. Corrections outside this range were made by linear extensions of the observed trends, with the incurred error included in the error limits (Table I). For all corrections, the difference in projectile mass is accounted for by considering cases at the same reduced energy (units of keV/amu).

B. Integrated total cross sections

For consistency, the total cross sections derived from integrating the DCSs to calculate values of ε can also be compared with experimental total cross sections. This requires one scaling constant, chosen here such that the value for He^{2+} + He at 2 keV/amu is equal to the average of the present total cross sections and those of Refs. [38,39]. It should be noted that the values presented here differ from those originally published [29]. This correction has been verified in correspondence with one of the authors [40].

C. Single electron capture results: He^{2+} + He

Shown in Fig. 5 is the energy dependence of σ_{21} for He^{2+} + He using the gas cells just discussed along with the lower-energy results of Okuno *et al.* [41] and Figueira da Silva *et al.* [42]. The octopole ion-beam guide [41] and double Faraday cup collision-cell arrangements [42] are able to accommodate the larger acceptance angles required at the lower energies. For example, the acceptance angle for the Vienna apparatus is 8° [42], and hence corrections have not been applied to these studies. Error bars shown are at the 2σ error limit, or 30% [43] for the data of Ref. [41]. Data of the present He-target measurements are listed in Table I.

The overall appearance of the resulting cross sections demonstrates good consistency among measurements of σ_{21} by five different experimental groups over a range of energies and techniques, as well as with the integrated results of B-MD. This is especially noteworthy given use of the less-forgiving linear cross-section scale. The acceptance-angle corrections introduced here significantly improve the agreement of the JPL results and those of Ref. [38]. At higher energies they

TABLE I. Absolute charge-exchange cross sections for $^3He^{2+}$ collisions with He and H_2. Units are 10^{-17} cm^2 for He, and 10^{-16} cm^2 for H_2 and D_2. Integral values for He and D_2 are from integrations of differential cross sections in Refs. [29] and [30], respectively. Errors are indicated at the 2σ level of uncertainty.

	He Single electron capture σ_{21}			H_2 and D_2 single electron capture σ_{21}		
Energy (keV/amu)	Uncorrected (10^{-17}cm^2)	Corrected (10^{-17}cm^2)	Integral Ref. [29]	Uncorrected (H_2) (10^{-16}cm^2)	Corrected (H_2) (10^{-16}cm^2)	Integral Ref. [30]
4.667	6.38	6.38 ± 0.54		4.88	5.05 ± 0.45	
2.667	5.31	5.31 ± 0.44		2.89	2.94 ± 0.25	
2.000	4.61	4.70 ± 0.38	5.2			3.1
1.500			4.2			3.0
1.333	3.90	4.20 ± 0.35		2.35	2.37 ± 0.25	
1.000	3.21	3.59 ± 0.28	3.3	2.15	2.18 ± 0.18	2.5
0.667	2.15	2.53 ± 0.23		2.26	2.30 ± 0.20	
0.500			3.7			
0.333	1.55	1.94 ± 0.33		2.28	2.34 ± 0.21	

also make consistent earlier measurements of Ref. [37]. The most recent measurements of Figueira da Silva *et al*. [42] are somewhat below other results, but are still in good agreement.

The convergence of experimental data from different laboratories enables one to make more critical comparisons with results of several theories (see Fig. 5). The semiclassical close-coupling, traveling atomic orbital (AO) theory of Fritsch [44] displays the correct slope down to its lower limit of 4 keV/amu, but is ∼20% below experimental values. The one-electron diatomic molecule orbitals (OEDM) approach

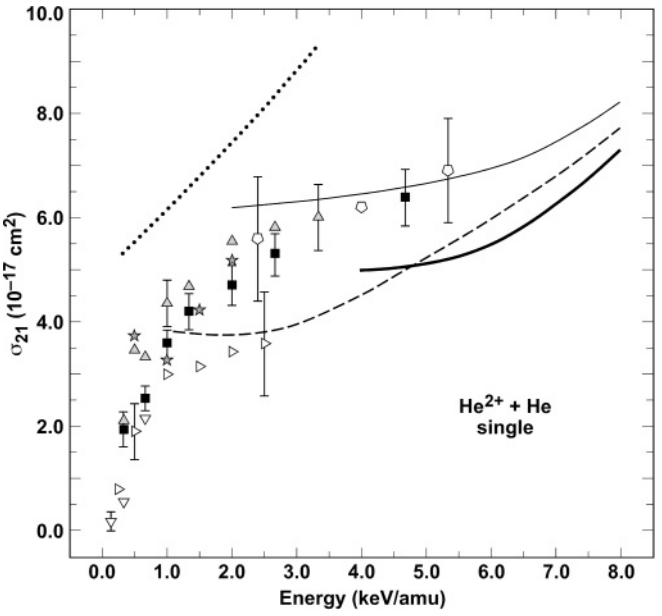

FIG. 5. Absolute single charge-exchange cross sections σ_{21} for $^3He^{2+}$ + He. Data are presented with 2σ error limits. The legend is ■, present JPL results, 1.93°, corrected; ▷, Figueira da Silva *et al*. [42]; △, Kusakabe *et al*. [38], corrected; ▽, Okuno *et al*. [41]; ★, Bordenave-Montesquieu and Dagnac [29], integrated; ⬡, Berkner *et al*. [37], corrected. The legend for results of theory is ——, Fritsch [44], close-coupling, traveling AO model; – – – –, Kimura [46], traveling MO theory; ——, Gramlich *et al*. [47], coupled-channel traveling AO theory; and • • • •, Schaudt *et al*. [48], time-dependent Hartree-Fock approach.

of Harel and Salin [45] (not shown) and a traveling MO approach of Kimura [46] agree with the Fritsch results and with each other. The Kimura results [46] extend to energies below 1 keV/amu. A separate coupled-channel traveling AO approach [47] gives results that are consistent with experiments for energies above 2 keV/amu. Finally, the time-dependent Hartree-Fock (TDHF) theory of Schaudt *et al*. [48] gives results that are monotonically increasing in the range 0.33–3.33 keV/amu (no evidence of a plateau region), and are a factor-of-2 higher than experiments. A classical quantum-coupling (CQC) enhancement at the lowest energy raises the cross section by 10%, making the agreement with experiments slightly worse [48].

Although not included here for the sake of clarity, the JPL studies were initially carried out for σ_{21} for He^{2+} + He using a gas cell with an acceptance angle of 0.60°. These values were consistently lower than those shown here by about 0.015 × 10^{-15} cm^2. The fact that the JPL- measured values increased significantly using a larger 1.20°-apertured cell gave the first experimental indication that collection-efficiency effects could be in play, which led to the decision to use the 1.93°-apertured collision cell.

In summary, for the energy range less than 2.5 keV/amu, without the present data and the additional integrated data of B-MD [29] one would be left with the diverging results of Kusakabe *et al*. [38] and Ref. [42]. One would be hard pressed to decide between them. In the range 2.5–5.5 keV/amu the JPL data at 2.67 and 4.67 keV/amu bracket and extend the data of Ref. [38], and the collection-efficiency corrections show that the data of Ref. [37] are indeed consistent. This encouraging consistency enables a clearer look at this low-energy region at higher magnification, with the good (factor-of-2) agreement of about 20 years ago replaced by a fairly divergent set of theoretical results, inviting renewed theoretical attention and deeper understanding of the basic processes at work.

D. Single electron capture results: He^{2+} + H_2

Replacing He with H_2 as the target provides a less demanding system in terms of acceptance angle. As shown in Fig. 6, present results and data from the other groups—including

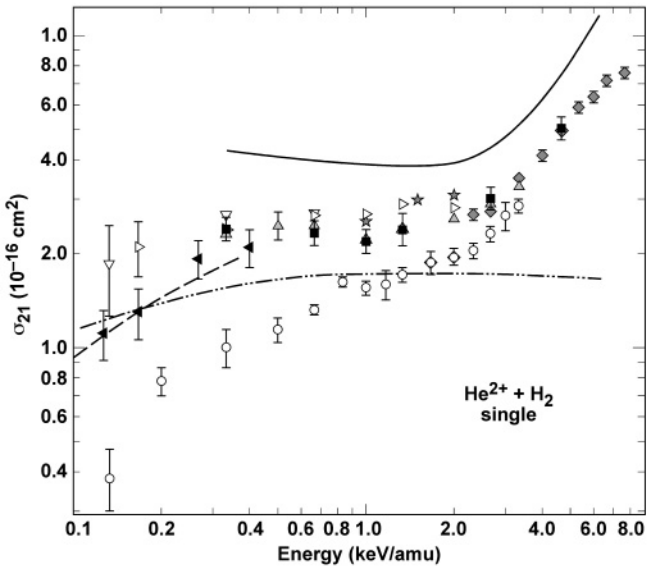

FIG. 6. Absolute single charge-exchange cross sections σ_{21} for $^3He^{2+} + H_2$. Data are presented with 2σ error limits. The legend for experimental results is ◀, Kusakabe *et al.* [39]; ▷, Figueira da Silva *et al.* [45]; ♦, Shah and Gilbody [46]; ∇, Okuno *et al.* [41]; △, Kusakabe *et al.* [38], corrected; ☆, Bordenave-Montesquieu and Dagnac [30], integrated; ○, Nutt *et al.* [47]; and ■, present results, 1.93°, corrected. The legend for results of theory is ———, Errea *et al.* [52], ten-state Franck-Condon model; — •• — •• —, Errea *et al.* [53], two-state vibrational excitation model; and — — —, Shimakura *et al.* [54], molecular-orbital expansion method.

those of Refs. [39,49]—are again consistent over a wide energy range. These also meet the data of Ref. [50] at energies above 2 keV/amu. Agreement is not as good, however, for the lower-energy data [51]. Although it is more difficult to use a gas-cell model for the open furnace-tube design [51] (used to facilitate the study of collisions with atomic hydrogen), in the intermediate energy range these data fall below the majority trend, analogous to the trend of data from the present 0.60°-apertured cell. The integrated cross sections of B-MD are also in agreement in this same region. This is significant as these data have been scaled to only the single He point. There is more scatter in the data at low energies, but agreement is again within error limits. Data of the present H_2-target measurements are also listed in Table I.

The overall shape of the curve is different for H_2, having a plateau over a broad energy range before rising steeply above 3 keV/amu. This increase is seen most clearly in the data of Ref. [50]; the JPL data point at 4.67 keV/amu agrees and is well above the plateau. The effect is described in the theoretical study of Errea *et al.* [52], and is apparent in their total cross-section results in their *ab initio* theory (Fig. 6). The sharp rise is attributed to the onset of nondissociative single electron capture (NDSEC). The nonvibrating Franck-Condon treatment of dissociative SEC (DSEC) overestimates this cross section in the lower-energy region ($E \leqslant 2$ keV/amu) [52]. However, results from a model with fewer states but including vibrational effects via the exit channel $He^+(1s) + H_2^+(2\sigma_g)$ [53] (shown as the —●●— line in Fig. 6) gives a value below experiment, with a shape that follows the experimental data. A detailed comparison with the assigned dissociative and nondissociative processes [30] could further illuminate these issues. More complete discussions of these theoretical results may be found in Refs. [52,53]. Finally, the molecular orbital expansion theory of Shimakura *et al.* [54] is in excellent agreement with the lowest-energy data. It reproduces the factor-of-2 drop in the cross section between 0.4 and 0.1 keV/amu and connects with the plateau.

In summary, at energies less than 0.4 keV/amu, there is good agreement among the results of theory [54], Kusakabe *et al.* [38], and the JPL results, but disagreement with the low values of Nutt *et al.* [51]. In the range 0.4–2.0 keV/amu, again in the absence of the present data and the integrated data of B-MD [29], one would have a high set of results [38,49] in contrast to a low set [51]. The present results and those of Ref. [29] confirm the higher values. The theoretical results of Errea *et al.* [52,53] with and without vibration sandwich the higher values, but differ by a factor of ≈2.5 from each other. At energies above 4 keV/amu, where the NDSEC channel is dominant, the JPL data extend to meet the experimental results of Ref. [50]. Results in the ten-state Franck-Condon model [52] are roughly 50% above experiments. Here again, given the accord in the experimental results, a reactivated approach to the theory of this multichannel problem would be illuminating.

E. Application to single electron capture for $He^{2+} + H_2O$ and CO_2

Earlier work of Ref. [36] dealing with acceptance-angle issues provides an excellent framework for extending the current benchmark results to other systems. For the case of elastic or near-elastic scattering of the fast He^{2+} projectile from the stationary target gas, the He^{2+} is confined to small-angle scattering [55]. Also, for small angles, the laboratory scattering angle θ_{lab} is related to the center-of-mass scattering angle $\theta_{c.m.}$ by $\theta_{lab} = m_{target}/(m_{target} + m_{projectile})\theta_{c.m.}$. Hence the laboratory scattering angles are larger for light projectiles on heavy targets. In this context it is also interesting to consider earlier measurements of single electron capture for $^3He^{2+}$ in the abundant cometary gas constituents H_2O [1,6] and CO_2 [1], especially at the lowest energies. In the case of H_2O, measurements down to 0.33 keV/amu using the larger 1.93° gas cell [6] extend earlier work [1] performed with the 1.20° cell into this interesting regime. Cross sections measured with the larger acceptance angle trend somewhat higher for the lowest two energy points where comparison can be made. Here it should be pointed out that the recommended total cross sections in Ref. [6] which go even lower in energy were predictions made to guide astrophysical plasma modelers on the basis of trends from the lowest-energy cross sections measured. The lowest of these nonmeasured values disagrees with the subsequent measurements of Seredyuk *et al.* [56], but as it is only a recommended value the experimental results do not disagree, and measured values in [6] and [56] are completely consistent.

For CO_2, which is more than twice as heavy as H_2O, we have measured a new low-energy data point for SEC with $^3He^{2+}$ using the 1.93° cell at 0.33 keV/amu, where we find $\sigma_{21} = 0.374(37) \times 10^{-15}$ cm^2. Extrapolating along the approximately linear decrease observed at low energy in Ref. [1], one obtains $\sigma_{21} \approx 0.29(5) \times 10^{-15}$ cm^2 at this energy.

Hence the new data point lies slightly above the extrapolated line but is in agreement within mutual uncertainties.

V. SUMMARY AND CONCLUSIONS

The present experimental results and discussions have given a framework to the absolute cross sections for charge exchange of He^{2+} with He and H_2. On the theoretical level, however, the situation is more uncertain, with room for significant improvement and hence improved understanding of the underlying atomic and molecular physics in both systems.

Furthermore, one would expect that the two-electron system $He^{2+} + H_2$ would be amenable to a variety of *ab initio* molecular-orbital calculations. But calculations for this system are made difficult by the presence of two Rydberg series $He(1s\,nl) + H_2{}^{2+}$ and $He^+(1s) + H_2{}^+(n\lambda)$ (where $n\lambda$ denotes the quantum state of the molecular electron), that present an infinity of excited states [52,53]. Calculations in a ten-state Franck-Condon [52] and two-state vibrational-excitation [53] approximation vary in magnitude but have the proper shapes for, respectively, the high- and low-energy regions of charge exchange. Outside these ranges both trend away from experiment (Fig. 6). Results of the ten-state calculation, moreover, indicate that DSEC is the dominant channel at low energy. While the model calculation of Ref. [54] agrees well with experiment below 0.4 keV/amu, the DSEC channel was omitted and led to the conclusion there that two-electron capture (TEC) is the dominant channel.

Beyond the cross sections themselves, aids to a more detailed understanding of the underlying processes include state-specific experimental energy-loss experiments [57], along with the B-MD measurements of He^+ angular differential cross sections that also identify the different reaction channels [29,30]. These data can serve to guide theory as to the relative importance of the NDSEC, DSEC, TEC, and Coulomb-explosion channels in the charge exchanges.

In conclusion, the question of angular acceptance in beam-gas studies of ion-molecule and ion-atom collisions has been studied in detail using the combination of a theoretical model [35], small-angle experimental DCSs [29,30], and fluid dynamic and molecular flow simulations of gas cells [33,34]. Fully stripped $^3He^{2+}$ is the lightest representative of the most abundant multiply-charged solar-wind ion. By measuring SEC cross sections in a variety of gas-cell geometries with benchmark H_2, exothermic He, and heavier targets H_2O and CO_2, angular acceptance effects have been observed and quantified for the lighter targets. These effects may also have relevance for studies of polyatomic species at low collision energies.

The model's efficacy has been demonstrated for H_2 and He by the improved consistency of data resulting from making small corrections amongst the various measured cross sections. These corrections are based on the low-angle DCSs and the specific geometries of the experimental gas-collision cells. Furthermore, limited studies of varying exit aperture size for the challenging cases of $^3He^{2+}$ collisions with heavy targets at very low energy can be interpreted as showing some small sensitivity in the expected direction.

From the understanding gained by the present results one may conclude that angular-acceptance effects should be essentially negligible in previous studies of the heavier and more highly charged (C, N, O, Ne, Fe)$^{q+}$ solar-wind ions at the higher energies ($\sim 2.5q$ and $7q$ keV) corresponding to slow and fast solar-wind velocities. These considerations will also apply to pending studies of highly charged Mg and Si ions. Taken together, these data will help interpret, for example, the successful EPOXI flyby of Comet Hartley-2 that detected CO_2 jets and H_2O vapor emanating from the comet surface [58].

ACKNOWLEDGMENTS

We thank C. R. Vane for informative discussions and for carrying out the alternative gas-cell effective-length calculation, and D. Bordenave-Montesquieu for providing differential cross sections in tabular form. We also thank L. Méndez for helpful discussions on the theory. This work was carried out at the Jet Propulsion Laboratory, California Institute of Technology and was supported through an agreement with the National Aeronautics and Space Administration.

[1] J. B. Greenwood, A. Chutjian, and S. J. Smith, Astrophys. J. **529**, 605 (2000).
[2] J. B. Greenwood, I. D. Williams, S. J. Smith, and A. Chutjian, Astrophys. J. Lett. **533**, L175 (2000).
[3] J. B. Greenwood, I. D. Williams, S. J. Smith, and A. Chutjian, Phys. Rev. A **63**, 062707 (2001).
[4] I. Čadež, J. B. Greenwood, A. Chutjian, R. J. Mawhorter, S. J. Smith, and M. Niimura, J. Phys. B **35**, 2515 (2002).
[5] I. Čadež, J. B. Greenwood, J. A. Lozano, R. J. Mawhorter, S. J. Smith, M. Niimura, and A. Chutjian, J. Phys. B **36**, 3303 (2003).
[6] J. B. Greenwood, R. J. Mawhorter, I. Čadež, J. Lozano, S. J. Smith, and A. Chutjian, Phys. Scr. T **110**, 358 (2004).
[7] R. J. Mawhorter, A. Chutjian, T. E. Cravens, N. Djurić, S. Hossain, C. M. Lisse, J. A. MacAskill, S. J. Smith, J. Simcic, and I. D. Williams, Phys. Rev. A **75**, 032704 (2007).
[8] N. Djurić, S. J. Smith, J. Simcic, and A. Chutjian, Astrophys. J. **679**, 1661 (2008).
[9] J. Simcic, D. R. Schultz, R. J. Mawhorter, I. Čadež, J. B. Greenwood, A. Chutjian, C. M. Lisse, and S. J. Smith, Phys. Rev. A **81**, 062715 (2010).
[10] J. Simcic, D. R. Schultz, R. J. Mawhorter, J. B. Greenwood, C. Winstead, B. V. McKoy, S. J. Smith, and A. Chutjian, Astrophys. J. **722**, 435 (2010).
[11] P. G. Carolan *et al.*, Phys. Rev. A **35**, 3454 (1987).
[12] S. Lepp, P. C. Stancil, and A. Dalgarno, J. Phys. B **35**, R57 (2002).
[13] R. C. Isler, Plasma Phys. Controlled Fusion **36**, 171 (1994).
[14] P. Beiersdorfer, M. Bitter, M. Marion, and R. E. Olson, Phys. Rev. A **72**, 032725 (2005).

[15] T. E. Cravens, Science **296**, 1042 (2002).
[16] V. A. Krasnopolsky, J. B. Greenwood, and P. C. Stancil, Space Sci. Rev. **113**, 271 (2004).
[17] C. M. Lisse *et al.*, Astrophys. J. **635**, 1329 (2005), and references therein.
[18] T. E. Cravens and T. I. Gombosi, Adv. Space Res. **33**, 1968 (2004).
[19] B. J. Wargelin and J. J. Drake, Astrophys. J. **578**, 503 (2002).
[20] R. F. Elsner *et al.*, J. Geophys. Res. **110**, A01207 (2005).
[21] V. Kharchenko, A. Dalgarno, D. R. Schultz, and P. C. Stancil, Geophys. Res. Lett. **33**, L11105 (2006).
[22] A. Bhardwaj *et al.*, Planet. Space Sci. **55**, 1135 (2007).
[23] N. A. Schwadron and T. E. Cravens, Astrophys. J. **544**, 558 (2000).
[24] K. Lodders and B. J. Fegley Jr., *The Planetary Scientist's Companion* (Oxford, New York, 1998).
[25] T. E. Cravens, Astrophys. J. **532**, L153 (2000).
[26] A. Chutjian, J. B. Greenwood, and S. J. Smith, in *Applications of Accelerators in Research and Industry*, edited by J. L. Duggan and I. L. Morgan (AIP, New York, 1999), p. 881.
[27] T. Ehrenreich, K. Miller, P. Gee, Q. Kessel, E. Pollack, W. W. Smith, N. Djurič, J. Lozano, S. J. Smith, and A. Chutjian, Nucl. Instrum. Methods Phys. Res. B **241**, 125 (2005).
[28] C. J. Verzani, K. Miller, A. Wrigley, Q. Kessel, W. W. Smith, S. J. Smith, S. Hossain, and A. Chutjian, Nucl. Instrum. Methods Phys. Res. B **261**, 189 (2007).
[29] D. Bordenave-Montesquieu and R. Dagnac, J. Phys. B **25**, 2573 (1992).
[30] D. Bordenave-Montesquieu and R. Dagnac, J. Phys. B **27**, 543 (1994).
[31] B. P. Mathur, J. E. Field, and S. O. Colgate, Phys. Rev. A **11**, 830 (1975).
[32] H. J. Blaauw, R. W. Wagenaar, D. H. Barends, and F. J. de Heer, J. Phys. B **13**, 359 (1980).
[33] See web location at http://www.ansys.com/products/simulations+technology/fluid+dynamics/Ansys+FLUENT.
[34] T. Haley, B.A. thesis, Pomona College, 2002.
[35] C. R. Vane (ORNL), private communication.
[36] R. E. Olson and M. Kimura, J. Phys. B **15**, 4231 (1982).
[37] K. H. Berkner, R. V. Pyle, J. W. Stearns, and J. C. Warren, Phys. Rev. **166**, 44 (1968).
[38] T. Kusakabe, H. Yoneda, Y. Mizumoto, and K. Katsurayama, J. Phys. Soc. Jpn. **59**, 1218 (1990).
[39] T. Kusakabe, Y. Miyamoto, M. Kimura, and H. Tawara, Phys. Rev. A **73**, 022706 (2006).
[40] D. Bordenave-Montesquieu, private communication.
[41] K. Okuno, K. Soejima, and Y. Kaneko, J. Phys. B **25**, L105 (1992).
[42] S. Figueira da Silva, G. Kowarik, F. Aumayr, and H. P. Winter, J. Phys. Conf. Ser. **58**, 181 (2007).
[43] K. Okuno, private communication.
[44] W. Fritsch, J. Phys. B **27**, 3461 (1994).
[45] C. Harel and A. Salin, J. Phys. B **13**, 785 (1980).
[46] M. Kimura, J. Phys. B **22**, L19 (1988).
[47] K. Gramlich, N. Grün, and W. Scheid, J. Phys. B **22**, 2567 (1989).
[48] K. J. Schaudt, N. H. Kwong, and J. D. Garcia, Phys. Rev. A **43**, 2294 (1991).
[49] S. Figueira da Silva, H. P. Winter, and F. Aumayr, Phys. Rev. A **75**, 042706 (2007).
[50] M. B. Shah and H. B. Gilbody, J. Phys. B **7**, 256 (1974).
[51] W. L. Nutt, R. W. McCullough, K. Brady, M. B. Shah, and H. B. Gilbody, J. Phys. B **11**, 1457 (1978).
[52] L. F. Errea, A. Macías, L. Méndez, B. Pons, and A. Riera, J. Phys. B **36**, L135 (2003).
[53] L. F. Errea, A. Macías, L. Méndez, B. Pons, and A. Riera, J. Chem. Phys. **119**, 325 (2003).
[54] N. Shimakura, M. Kimura, and N. F. Lane, Phys. Rev. A **47**, 709 (1993).
[55] H. Goldstein, in *Classical Mechanics*, 2nd ed. (Addison-Wesley, Boston, MA, 1980), p. 118.
[56] B. Seredyuk *et al.*, Phys. Rev. A **71**, 022705 (2005).
[57] J. M. Hodgkinson, T. K. McLaughlin, R. W. McCullough, J. Geddes, and H. B. Gilbody, J. Phys. B **28**, L393 (1995).
[58] See http://stardustnext.jpl.nasa.gov/mission/cosmicsnow.html, and a review by M. R. Combi *et al.*, Astron. J. **141**, 128 (2011).